Instability of a Mixed Layer Model and the Generation of Near-Inertial Motion. Part II: Mixed Layer Deepening

JOHN KROLL

Department of Mathematical Sciences, Old Dominion University, Norfolk, Virginia

(Manuscript received 18 November 1986, in final form 11 December 1987)

ABSTRACT

In Part I we examined the stability of a model of the mixed layer, neglecting the deepening rate. Here we examine the effects of the deepening but neglect the oscillations in the steady state. We find that the two types of instability found previously are modified. The long wavelength [O(10) km] instability becomes more stable while the converse is true for the short wavelength [O(1) km] instability with the purely kinematic effect of the slowly deepening mixed layer on the equally slow vertically propagating near-inertial waves being of most importance. The short wavelength instability might be expected to be observed if the lateral friction is sufficiently large. There is also a different short wavelength instability which is basically independent of the ocean interior which might be expected to appear if friction is sufficiently small.

1. Introduction

In the previous paper (Kroll 1988, denoted as Part I hereafter) we investigated the stability of a mixed layer deepening model. There we assumed that the deepening rate was negligible and found two basic instability mechanisms. The first, a viscous parallel flow type, was characterized by a relatively short wavelength with the most unstable wave directed generally along the steady mean flow. The second, an inflection point type, was characterized by a relatively long wavelength with the most unstable wave directed generally against the wind at a right angle to the mean flow. The first had been investigated previously (Kroll 1982, 1984) and the second by Stern (1977) and Kamachi and Grimshaw (1984). Thus the present model has brought both mechanisms within the same model.

In this paper we will consider the effects of deepening. The solutions of Part I will then be modified by effects from the heat equation and the turbulent kinetic energy (TKE) equation. Of at least equal importance is the purely kinematic effect of the slow moving boundary on the similarly slow vertical propagation of near-inertial waves. We will also investigate instabilities not present in Part I.

At this time we are seeking to solve the problem analytically, so we must simplify somewhat. We cannot consider deepening and steady-state oscillations simultaneously, so we will examine a steady mean flow only. After the initially rapid deepening, the relatively slow deepening thereafter is not constant, but we will assume it is constant.

2. The basic equations

From Part I the dimensionless perturbation equations for the mixed layer from the perturbation of the Niiler deepening model (1975) and modified by de-Szoeke (1980) are

$$\mathbf{u}_t + R\bar{u}\mathbf{u}_x + \mathbf{k}f\times\mathbf{u} = -p_x\mathbf{i} - h(\boldsymbol{\tau}_0 - \bar{h}_t\bar{\mathbf{u}})/\bar{h}^2 - \bar{\mathbf{u}}H/\bar{h} - \bar{h}_t\Delta\mathbf{u}/\bar{h} + \sigma\mathbf{u}_{xx} + E\mathbf{u}_{zz} - \frac{\bar{\sigma}}{\bar{h}}(|\bar{\mathbf{u}}|\mathbf{u} + (\mathbf{u}\cdot\mathbf{u})\bar{\mathbf{u}}/|\bar{\mathbf{u}}| - h|\bar{\mathbf{u}}|\bar{\mathbf{u}}/\bar{h}) \quad (1a)$$

$$p_z = RT \quad (1b)$$

$$T_t + R\bar{u}T_x = -h(bQ_0 - \overline{\Delta T}\bar{h}_t)/\bar{h}^2 - (\bar{h}_t\Delta T + \overline{\Delta T}H)/\bar{h} + \sigma T_{xx} + ET_{zz} \quad (1c)$$

$$(\bar{h}\overline{\Delta T} - |\bar{\mathbf{u}}|^2)H + \bar{h}_t(\bar{h}\Delta T + \overline{\Delta T}h - 2\bar{\mathbf{u}}\cdot\Delta\mathbf{u}) = -bQ_0h + 2\int_{-\bar{h}}^{0}(\boldsymbol{\tau}_0 + z(\boldsymbol{\tau}_0 - \bar{h}_t\bar{\mathbf{u}})/\bar{h})\cdot\mathbf{u}_z dz \quad (1d)$$

$$u_x + w_z = 0 \quad (1e)$$

where the overbar represents a mean or unperturbed quantity, the variables and parameters are defined in Table 1, and the viscous dissipation ϵ has been neglected. (As before, we have included both horizontal eddy viscosity and mean-square drag, the former to deal with short wavelengths and the latter for long wavelengths.) The interface parameter H is continuous across the interface at $z = -\bar{h}$ (as is h) and given by

$$H = [h_t + R(\bar{u}h_x + w)]_+ = (h_t + Rw)_- \quad (2)$$

Corresponding author address: Prof. John E. Kroll, Dept. of Mathematical Sciences, Old Dominion University, Norfolk, VA 23508-8527.

© 1988 American Meteorological Society

Unauthenticated | Downloaded 01/15/25 02:54 PM UTC

TABLE 1. Dimensionless variables and parameters.

x	horizontal coordinate, direction of perturbation wave, nondimensionalized by L = 1 km
z	upward coordinate, nondimensionalized by $h_* = u_*/(N_- f_0)^{1/2}$, where $u_* = (\tau^0/\rho_0)^{1/2}$, N_- is N below the mixed layer, and τ^0 is the magnitude of the stress at the surface
t	time, nondimensionalized by $1/f_0$
$\mathbf{u}$	(u, v), the horizontal perturbation velocity, nondimensionalized by $U_0 = \tau^0/f_0 h_* \rho_0$
f	dimensionless inertial frequency = 1
w	vertical perturbation velocity, nondimensionalized by $U_0 h_*/L$
p	perturbation pressure, nondimensionalized by $\rho_0 f_0 U_0 L$
T	perturbation temperature, nondimensionalized by $h_* \Gamma$, $\Gamma = dT/dz = N_-^2/\alpha g$ where α = the coefficient of thermal expansion
h	perturbation depth of the mixed layer, nondimensionalized by h_*; $\bar{h}$ is the mean depth
θ	angle between direction of the wind and the wave perturbation (the x-axis)
ω	wave frequency = $\omega_r + i\omega_i$, nondimensionalized by f_0; ω_m is the mixed layer frequency
k	horizontal wavenumber, nondimensionalized by $1/L$
μ	vertical wavenumber in the interior = $Rk/(\omega^2 - f^2)^{1/2}$, $f = 1$
ΔT	temperature jump across transition layer for the mean state
R	$U_0/f_0 L$ is the Rossby number
σ	$K_H/f_0 L^2$ is the horizontal Ekman number, assumed the same for heat
$\bar{\sigma}$	$N_- C/f_0$, a horizontal drag coefficient. C is the usual coefficient
E	$K_v/f_0 h_*^2$ is the vertical Ekman number, assumed the same for heat
b	$\alpha g Q^0/u_*^2 N_-$, heating coefficient. Q^0 is the magnitude of the surface heating
$\bar{h}_t$	mean deeping rate
τ_0	applied surface stress nondimensionalized by τ
Q_0	applied surface heating nondimensionalized by Q^0

where + and − subscripts denote top and bottom of the transition layer respectively.

Assuming a constant buoyancy frequency, N_-, the dimensionless interior equations are

$$\mathbf{u}_t + \mathbf{k}f \times \mathbf{u} = -(p_x - R\overline{\Delta T} h_x)\mathbf{i} \tag{3a}$$

$$p_z = RT \tag{3b}$$

$$T_t + Rw = 0 \tag{3c}$$

$$u_x + w_z = 0. \tag{3d}$$

From Part I for the steady state we have

$$\bar{\mathbf{u}} = \tau_0(\sin\theta, -\cos\theta)/f\bar{h} = (\bar{u}, \bar{v}) \tag{4}$$

and $\overline{\Delta T}$ can be found from Eq. (15) in Part I, but we will examine various values, using, as a rule, the nominal value $\overline{\Delta T} = 0.5\bar{h}$. We will also consider various values for $\bar{h}_t$ but ultimately consider realistic values which are consistent with Eq. (8c) in Part I given approximately by

$$\bar{h}_t \approx 2(n_G - n_D)(N_-/f_0)^{-1/2}(\bar{h}\overline{\Delta T} - |\bar{\mathbf{u}}|^2)^{-1}$$
$$\approx 0.5/(\bar{h}\overline{\Delta T} - |\bar{\mathbf{u}}|^2) \tag{5}$$

and $\bar{h}\overline{\Delta T} - |\bar{\mathbf{u}}|^2 > 0$.

The boundary conditions again are that at $z = 0$: $\mathbf{u}_z = T_z = w = 0$ and at $z = -\bar{h}(t)$, p and $uh_x + w$ are continuous and $\mathbf{u}_z = T_z = 0$. Also we need the radiation condition that no energy is coming from $z \to -\infty$.

3. The solution

We are assuming $\bar{h}(t)$ varies only slowly in t (i.e., $\bar{h}_t/\bar{h} \ll f$) and can be considered constant everywhere except when the frequencies of the mixed layer and the interior are matched at $z = -\bar{h}(t)$ where we will assume $\bar{h} = \bar{h}_0 + \bar{h}_t t$ with $\bar{h}_t$ constant.

We can show that T and H are uniform in z from (1c, d) so that p is linear in z and hence $\mathbf{u}$ in (1a) will not be uniform in z. We assume a solution in the form $\hat{(\ )}e^{ikx - i\omega_m t}$, where ω_m is the frequency in the mixed layer, and assume $\hat{\mathbf{u}} = \hat{\mathbf{u}}_1 + \hat{\mathbf{u}}_2(z)$, a partition in uniform and varying parts. For the varying part of (1a) we have

$$iq\hat{u}_2 - f\hat{v}_2 = -ikR\hat{T} \cdot (z + \bar{h}) + E\hat{u}_{2_{zz}} \tag{6a}$$

$$iq\hat{v}_2 + f\hat{u}_2 = E\hat{v}_{2_{zz}} \tag{6b}$$

where $q = Rk\bar{u} - \omega_m - i\sigma k$, and we have neglected the drag, $\bar{\sigma}$, which simplifies the results considerably. This simplification seems valid because it happens that the z-dependent solution has more effect for short wavelengths which are relatively unaffected by the drag. Equations (6) can most easily be solved by letting $\psi = \hat{u}_2 + i\hat{v}_2$, $\phi = \hat{u}_2 - i\hat{v}_2$ to obtain

$$E\psi_{zz} - i(q + f)\psi = ikR\hat{T} \cdot (z + \bar{h}) \tag{7a}$$

$$E\phi_{zz} - i(q - f)\phi = ikR\hat{T} \cdot (z + \bar{h}) \tag{7b}$$

which can be easily solved using the boundary conditions $\hat{\mathbf{u}}_{2_z} = 0$ at $z = 0, -\bar{h}$ to obtain

$$\begin{pmatrix} \hat{u}_2(z) \\ \hat{v}_2(z) \end{pmatrix} = \begin{pmatrix} U_2(z) \\ V_2(z) \end{pmatrix} \hat{T}$$

where

$$\begin{pmatrix} U_2(z) \\ V_2(z) \end{pmatrix} = \begin{pmatrix} 1 \\ -i \end{pmatrix} \frac{kR}{2} \left\{ \left[\frac{(\cosh m\bar{h} - 1)\cosh mz}{m(q+f)\sinh m\bar{h}} + \frac{\sinh mz}{m(q+f)} \right] + \left[\frac{(\cosh m'\bar{h} - 1)\cosh m'z}{m'(q-f)\sinh m'\bar{h}} + \frac{\sinh m'z}{m'(q-f)} \right] + \begin{pmatrix} -q \\ f \end{pmatrix} \frac{2(z + \bar{h})}{q^2 - f^2} \right\} \tag{8}$$

and

$$\begin{pmatrix} m \\ m' \end{pmatrix} = (i(q \pm f)/E)^{1/2}.$$

The effect of this variable part on the remainder of the system is most significant through the stress working term in the TKE equation which is the integral in (1d), and on w in the continuity equation. We can show that the integral in (1d) is given by

Unauthenticated | Downloaded 01/15/25 02:54 PM UTC

$$\boldsymbol{\tau}_0 \cdot \left(\hat{\mathbf{u}}_2(0) - (1/\bar{h})\int_{-\bar{h}}^{0} \hat{\mathbf{u}}_2 dz\right) - \bar{h}_t \hat{\mathbf{u}} \cdot \left(\hat{\mathbf{u}}_2(-\bar{h}) - (1/\bar{h})\int_{-\bar{h}}^{0} \hat{\mathbf{u}}_2 dz\right). \quad (9)$$

From (1e) we have

$$\hat{w}(-\bar{h}) \equiv \hat{w}_+ = ik\left(\bar{h}\hat{u}_1 + \int_{-\bar{h}}^{0} \hat{u}_2 dz\right). \quad (10)$$

Equations (1c) and (1d) can be solved simultaneously using (8) and (9) yielding to lowest order in $\bar{h}_t$:

$$\hat{T} = 2\bar{h}_t[\bar{u}(\hat{u}_1 - \hat{u}_-) + \bar{v}(\hat{v}_1 - \hat{v}_-) + \overline{\Delta T}\hat{h}]/\bar{h}^2 D \quad (11)$$

where $D = iq + 2\tau_0(\cos\theta(U_2(0) - \langle U_2\rangle) + \sin\theta(V_2(0) - \langle V_2\rangle))/\bar{h}^2$ and where

$$(\langle U_2\rangle, \langle V_2\rangle) \equiv (1/\bar{h})\int_{-\bar{h}}^{0} (U_2, V_2) dz = -0.5kR\bar{h}(q, if)/(q^2 - f^2); \quad (12)$$

$\hat{H}$ is similar but more complicated. The $\hat{T}$ and $\hat{H}$ are order $\bar{h}_t$ as long as D is O(1). For D vanishing, we obtain what we call the internally dominant solution which we will discuss later.

Using the previous results for the z-dependent part in the uniform part we obtain from (1a, b, c, d):

$$(iq_1 + \bar{h}_t/\bar{h})\hat{u}_1 - f_1\hat{v}_1 = -ik\hat{p}_+ - T_u\hat{h}/\bar{h}^2 - \bar{h}_t U_1(-\bar{h})\frac{\hat{T}}{\bar{h}} + \bar{h}_t\hat{u}_-/\bar{h} \quad (13a)$$

$$(iq_2 + \bar{h}_t/\bar{h})\hat{v}_1 + f_2\hat{u}_1 = -T_v\hat{h}/\bar{h}^2 - \bar{h}_t V_1(-\bar{h})\frac{\hat{T}}{\bar{h}} + \bar{h}_t\hat{v}_-/\bar{h} \quad (13b)$$

$$(iq + \bar{h}_t/\bar{h})\hat{T} = -\overline{\Delta T}\hat{H}/\bar{h} + \bar{h}_t\hat{T}_-/\bar{h} - (bQ_0 - \overline{\Delta T}\bar{h}_t)\hat{h}/\bar{h}^2 \quad (13c)$$

$$(\bar{h}\overline{\Delta T} - |\bar{\mathbf{u}}|^2)\hat{H} = 2(A_\tau + \bar{h}_t A_u)\hat{T} - (bQ_0 + \overline{\Delta T}\bar{h}_t)\hat{h} + \bar{h}_t\bar{h}\hat{T}_- + 2\bar{h}_t(\bar{u}\hat{u}_1 + \bar{v}\hat{v}_1 - \bar{u}\hat{u}_- - \bar{v}\hat{v}_-), \quad (13d)$$

where $q_{1,2} = q - i\bar{\sigma}\tau_0(\frac{3}{2} \mp \cos(2\theta)/2)f\bar{h}^2$, $f_{1,2} = f \pm \bar{\sigma}\tau_0 \sin(2\theta)/2f\bar{h}^2$, $T_u = \tau_0\cos\theta - \bar{h}_t\bar{u} - \bar{\sigma}|\bar{\mathbf{u}}|\bar{u}/\bar{h}^2$, $T_v = \tau_0\sin\theta - \bar{h}_t\bar{v} - \bar{\sigma}|\bar{\mathbf{u}}|\bar{v}/\bar{h}^2$, $A_\tau = \tau_0\cos\theta(U_1(0) - \langle U_1\rangle) + \tau_0\sin\theta(V_1(0) - \langle V_1\rangle)$, and $A_u = \bar{u}\langle U_1\rangle + \bar{v}\langle V_1\rangle - h/2$. From (2) and (10), we have

$$i\omega_m\hat{h} = R\hat{w}_- - \hat{H} \quad \text{and,} \quad (14)$$

$$\hat{w}_- - ik\hat{u}\bar{h} = ik\bar{h}(\hat{u}_1 + \langle U_1\rangle\hat{T}). \quad (15)$$

We find $\hat{u}_-$, $\hat{v}_-$, $\hat{w}_-$ and $\hat{T}_-$ from the solution of the equation set (3) for the interior. Similarly to Kroll (1982), we find

$$p - R\overline{\Delta T}h = Pe^{i\mu\bar{h}_0}e^{i(kx+\mu z-\omega t)} \quad (16)$$

where $\mu^2 = k^2R^2/(\omega^2 - f^2)$ and ω is the frequency in the interior. We are assuming that $\bar{h}(t)$ is essentially constant except for the matching at the interface $z = -\bar{h}(t) = -(\bar{h}_0 + \bar{h}_t t)$ where $\bar{h}_t \ll 1$ and constant. (To lowest order for this matching, the mixed layer can be assumed to be independent of z.) Then (16) at the interface becomes

$$p_- - R\overline{\Delta T}h = Pe^{ikx - i(\omega + \bar{h}_t\mu)t}. \quad (17)$$

So for the frequencies in the mixed layer and interior to match, we must have

$$\omega_m = \omega + \bar{h}_t\mu. \quad (18)$$

Using (16) in the set (3) and evaluating at $z = -\bar{h}(t)$, we find

$$\hat{u}_- = \omega kP/(\omega^2 - f^2), \quad \hat{v}_- = -ikfP/(\omega^2 - f^2), \quad \hat{w}_- = -\omega\mu P/R^2 \quad \text{and} \quad \hat{T}_- = i\mu P/R. \quad (19)$$

Continuity of pressure implies

$$\hat{p}_+ = P + R\overline{\Delta T}\hat{h}. \quad (20)$$

Eliminating $\hat{p}_+$, $\hat{u}_-$, $\hat{v}_-$, $\hat{w}_-$ and $\hat{T}_-$, Eqs. (13) through (15) constitute a system of six equations and six unknowns, $\hat{u}_1$, $\hat{v}_1$, $\hat{h}$, $\hat{H}$, $\hat{T}$ and P, whose determinant set to zero is the eigenvalue equation for ω. What we call the externally dominant solution is the solution of Part I which has trivial solutions for $\hat{H}$ and $\hat{T}$ for $\bar{h}_t = 0$ which is now modified for $\bar{h}_t > 0$. The internally dominant solution mentioned earlier is not trivial for $\hat{H}$ and $\hat{T}$. In the next two sections we will discuss these two classes.

We have not systematically investigated the effects of heating, so we will assume $bQ_0 = 0$ in what follows. From limited calculations, it appears that heating is most important in how it affects $\overline{\Delta T}$ in the steady state with surface cooling (heating), producing a decrease (increase) in $\overline{\Delta T}$, being destabilizing (stabilizing).

4. Kinematics of the deepening interface

Before proceeding to specific solutions, equation (18) bears further examination. It represents a Doppler effect type of frequency variation due to a moving source. However, the behavior is not that of simple plane waves since inertio–gravity waves have their own unique character. Let us consider again (18), substituting for μ:

$$\omega_m = \omega + \bar{h}_t kR(\omega^2 - f^2)^{-1/2} \quad (21)$$

where ω and ω_m are complex in general. Figure 1 represents the mapping between the complex ω and complex ω_m planes for $\mathrm{Re}(\omega)$, $\mathrm{Re}(\omega_m) \geq 0$, using the correct branch of the radical to ensure downward radiation. (We have symmetry about the imaginary axes for $\mathrm{Re}(\omega)$, $\mathrm{Re}(\omega_m) < 0$.) On the ω-plane the region outside ACBA and the region inside ACBA each map onto the

Unauthenticated | Downloaded 01/15/25 02:54 PM UTC

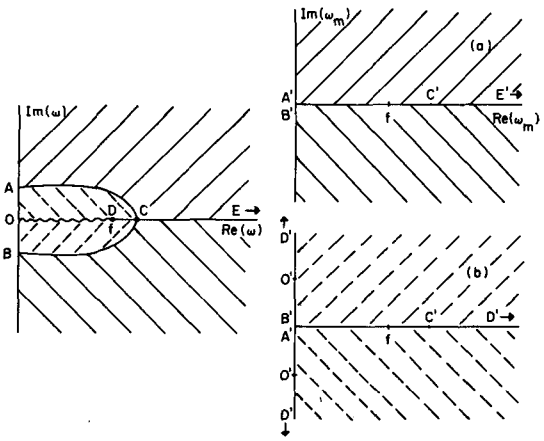

FIG. 1. The mapping between the complex-ω (left) and complex-ω_m (right) planes from Eq. (21). The region outside (inside) ACBA on the ω-plane maps onto sheet (a) (sheet (b)) of the ω_m-plane. Corresponding mapped areas have the same shading. Outside (inside) ACBA ($c_{g_z} - \bar{h}_t$) is >0 (<0) and is 0 on the boundary ACB.

entire ω_m half-plane with the former mapped onto sheet (a) and the latter onto sheet (b). The point C is the critical point of the mapping where $d\omega_m/d\omega = 0$, which yields from (21), $(\omega^2 - f^2)^{3/2}/\omega kR = \bar{h}_t$. For real ω, the left side of this equation is the dimensionless downward vertical group speed, c_{g_z}. Furthermore, we can show $c_{g_z} = \bar{h}_t$ on the curves AC and BC [using c_{g_z} = (downward energy flux)/(total energy density) $= 2\,\mathrm{Re}(\omega\mu)\,|\omega^2 - f^2|^2/R^2k^2(|\omega|^2 + f^2 + |\omega^2 - f^2|)$ for complex ω] and $c_{g_z} - \bar{h}_t > 0$ outside ACBA and <0 inside ACBA.

The imaginary parts, $\mathrm{Im}(\omega) \equiv \omega_i$ and $\mathrm{Im}(\omega_m) \equiv \omega_{m_i}$, are of particular interest. Solutions associated with sheet (a) on the ω_m-plane must have $c_{g_z} \geqslant \bar{h}_t$ and both ω_{m_i} and $\omega_i \geqslant 0$ or both ω_{m_i} and $\omega_i \leqslant 0$. The system is clearly unstable for the former and stable for the latter (or neutral for equalities). Solutions associated with sheet (b) on the ω_{m_i}-plane must have $c_{g_z} \leqslant \bar{h}_t$ and $\omega_{m_i} \geqslant 0$, $\omega_i \leqslant 0$ or $\omega_{m_i} \leqslant 0$, $\omega_i \geqslant 0$. The interpretation of this case is not as clear.

For $\omega_{m_i} > 0$ and $\omega_i < 0$, one could visualize the amplitude in the mixed layer growing while that in the interior was stable for sufficiently rapid deepening. On the other hand for $\omega_{m_i} < 0$ and $\omega_i > 0$, we argue that the system is stable, even though $\omega_i > 0$, because the energy source is in the mixed layer and the motion is stable there with no energy leaving the interface into the interior. This situation is realizable if we have a downward advecting stable field fixed with respect to the downward moving boundary. If the field decreases with depth [$\mathrm{Im}(\mu) < 0$], then $\omega_i = \omega_{m_i} - \bar{h}_t\,\mathrm{Im}(\mu)$ could be positive even though the system is stable. An observer at a fixed point z would see the amplitude of the field increase but only until the interface reached that point.

5. Specific solutions

a. Externally dominant class

We assume D in (11) is O(1) so that $\hat{T}$ (and $\hat{H}$) are $O(\bar{h}_t)$. We want to see how increasing $\bar{h}_t$ affects our long and short wavelength instabilities of Part I. We want conditions where both instabilities are present, but we cannot consider $\Delta T = 0$ as we did there since it violates (5). To have $\bar{h}_t \ll 1$ and to be also consistent with the model, we should have $\bar{h}\Delta T - |\bar{\mathbf{u}}|^2 \gg 0$ from (5), but we will relax this constraint to examine the tendencies of the solutions. We choose points on Fig. 7 of Part I for $\Delta T = 0.1$ where $\omega = (0.986, 0.006)$ for the long-wave and $\omega = (2.10, -0.27)$ (off the graph) for the short-wave instability. We solve the system of equations (13) through (15) [assuming $\bar{h}\Delta T - |\bar{\mathbf{u}}|^2 \approx \bar{h}\Delta T$ in (13d)] and obtain Fig. 2 showing the effect of increasing $\bar{h}_t$.

Based on our analysis and discussion of Fig. 1, we assume our system is unstable only if $\omega_{m_i} > 0$. So we have plotted ω_{m_i} versus $\bar{h}_t$. For the short wave curve, ω_i and ω_{m_i} have the same sign so that where this curve crosses the $\bar{h}_t$-axis the solution is crossing the $\mathrm{Re}(\omega)$ axis on Fig. 1 for $\mathrm{Re}(\omega) > C$. For the long-wave curve, where the curve crosses the $\bar{h}_t$-axis the sign of ω_i remains positive and on Fig. 1 the solution is crossing the curve AC. Clearly the long instability tends to be stabilized and the short one destabilized by increasing $\bar{h}_t$ which seems to be true in general.

In addition to our modified long- and short-wave solutions there is a solution that exists only for $\bar{h}_t > 0$, which is not shown. It corresponds to the case on Fig. 1 where $\omega_{m_i} > 0$ and $\omega_i < 0$ with c_{g_z} always $\leqslant \bar{h}_t$. An analysis of the reflection problem, where ω and ω_m are real, indicates that the solution corresponding to this case has zero amplitude. So for the initial value problem associated with this stability problem, such an instability may not be significant. At any rate we will not analyze this solution in any detail since we are primarily interested in the propagation of waves into the interior at this time.

An examination of the terms of the eigenvalue equation as $\bar{h}_t$ is increased reveals that the purely kinematic effect of the moving interface seems the most important; i.e., Eq. (18). Even for $\bar{h}_t$ small, ω_m can differ greatly from ω because μ is large for near-inertial motion (∞ for exactly inertial) or for Rk large. Another important effect is the interaction of the deepening and the jump in the perturbation velocity across the interface from the $\bar{h}_t\Delta\mathbf{u}$ term in (1a). This term is of order $\bar{h}_t(\omega^2 - f^2)^{-1}$ which is order one or larger for near-inertial motion. This term is important for the instability mentioned here that exists only for $\bar{h}_t > 0$. The terms resulting from the z-dependent part of the solution seem to be less important.

As in Part I, the short-wave instability is strongly stabilized by increasing ΔT, but so is the long-wave instability which was not the case previously. This is

Unauthenticated | Downloaded 01/15/25 02:54 PM UTC

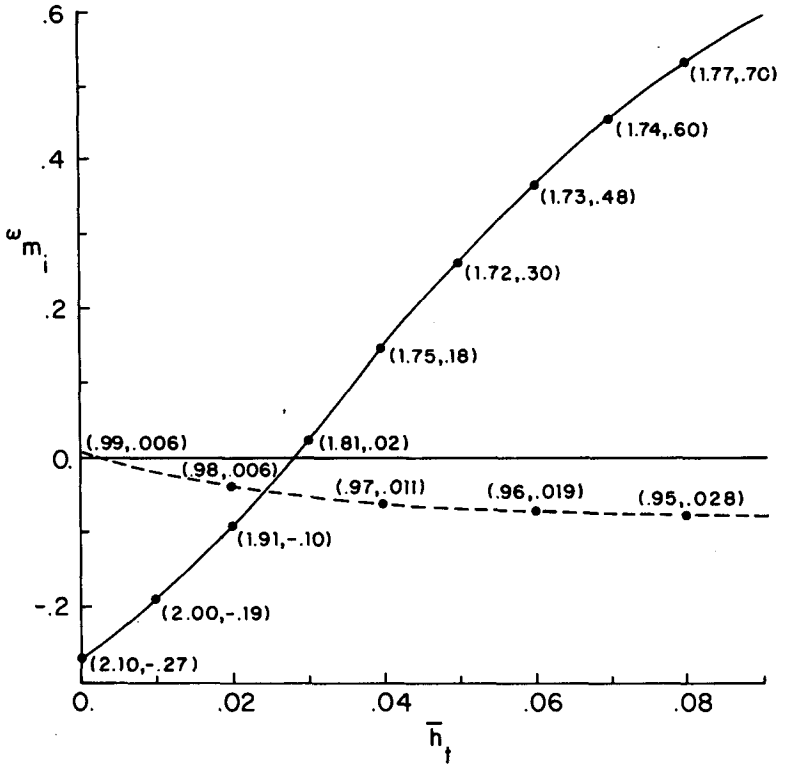

FIG. 2. The imaginary part of the mixed layer frequency (ω_{m_i}) vs the deepening rate ($\bar{h}_t$) for the short wave instability (solid curve) for $\theta = 92°$ and $k = 4.0$ and the long wave instability (dashed curve) for $\theta = 198°$ and $k = 0.22$ with $R = \bar{h} = 2.0$, $\overline{\Delta T} = 0.1$, $\sigma = 1.0$, $\bar{\sigma} = 0.1$, and $E = 1.0$. The complex frequency in the interior (ω) is in parentheses.

illustrated on Fig. 3 where ω_{m_i} is plotted versus $\overline{\Delta T}$ for $\bar{h}_t$ fixed. Note that the portion of each curve where $\omega_{m_i} < 0$ is stable even though $\omega_i > 0$ because the vertical group speed is less than the deepening rate as previously explained. The little peak in the short wave curve is stable in the interior ($\omega_i < 0$) but unstable in the mixed layer ($\omega_{m_i} > 0$). Thus the mixed layer would be unstable but not radiate waves. The path of this loop can be traced on Fig. 1 where it goes through C at $\omega = (1.27, 0.0)$, dips below the Re(ω) axis and recrosses that axis between D and C at $\omega = (1.30, 0.0)$.

For a realistic temperature jump, $\overline{\Delta T} \approx 0.5\bar{h}$, Fig. 3 indicates that no instability would be expected. We can have the short wave instability if we relax ΔT as illustrated in (θ, k) space on Fig. 4 for $\overline{\Delta T} = 0.2$. The interior is unstable with a group speed greater than the deepening rate only in the small area shown which is also the only region where $\omega_{m_i} > 0$. This region disappears quickly with increasing $\overline{\Delta T}$. In this case $(\bar{h}\overline{\Delta T} - |\bar{\mathbf{u}}|^2)$ is small and $\bar{h}_t$ would be unrealistically large unless there were significant surface cooling [see (8c) of Part I]. We thus conclude that within the region of applicability of the model, for the canonical values of the parameters, unstable waves are unlikely for a deepening mixed layer. (The canonical values are $\overline{\Delta T} = 1.0$, $R = \bar{h} = 2.0$, $\bar{h}_t = 0.05$, $\bar{\sigma} = 0.1$, $\sigma = 1.0$ and $E = 1.0$, based on $\tau^0/\rho_0 = 2\ \text{cm}^2\ \text{s}^{-2}$, $N_-/f_0 = 200$, $f_0 = 10^{-4}\ \text{s}^{-1}$, $K_H = 10^6\ \text{cm}^2\ \text{s}^{-1}$, $K_v = 10^2\ \text{cm}^2\ \text{s}^{-1}$, $L = 1$ km and $C = 0.5 \times 10^{-3}$.)

However, if we assume K_H is two orders of magnitude greater, i.e., $O(10^8\ \text{cm}^2\ \text{s}^{-1})$ rather than $O(10^6\ \text{cm}^2\ \text{s}^{-1})$, we can obtain realistic results. Figure 5 shows how ω_{m_i} actually increases for increasing $\sigma = K_H/f_0L^2$. As before, the group speed is greater than the deepening rate only for $\omega_{m_i} > 0$. So only that portion of the curve above zero is unstable. If we start at the point on this figure where $\sigma = 100$ and decrease $\bar{h}_t$, we obtain the curve on Fig. 6. If we take the point on that curve where $\bar{h}_t = 0$ and decrease σ continuously to 1.0 and $\overline{\Delta T}$ to 0.0, we obtain a point on Fig. 2 of Part I for the short-wave instability. So the solution we are considering is a continuation of the short-wave instability for increasing σ, $\overline{\Delta T}$ and $\bar{h}_t$.

The origin of this instability can be seen by going back to Eqs. (13) through (20). If we let σ become large, which means q_1, q_2 and q become large, then from (13a, b, c) $\hat{u}_1$, $\hat{v}_1$ and $\hat{T}$ become small. The $\hat{H}$ from (13d) will be $O(\bar{h}_t)$, assuming $b = 0$, and the

Unauthenticated | Downloaded 01/15/25 02:54 PM UTC

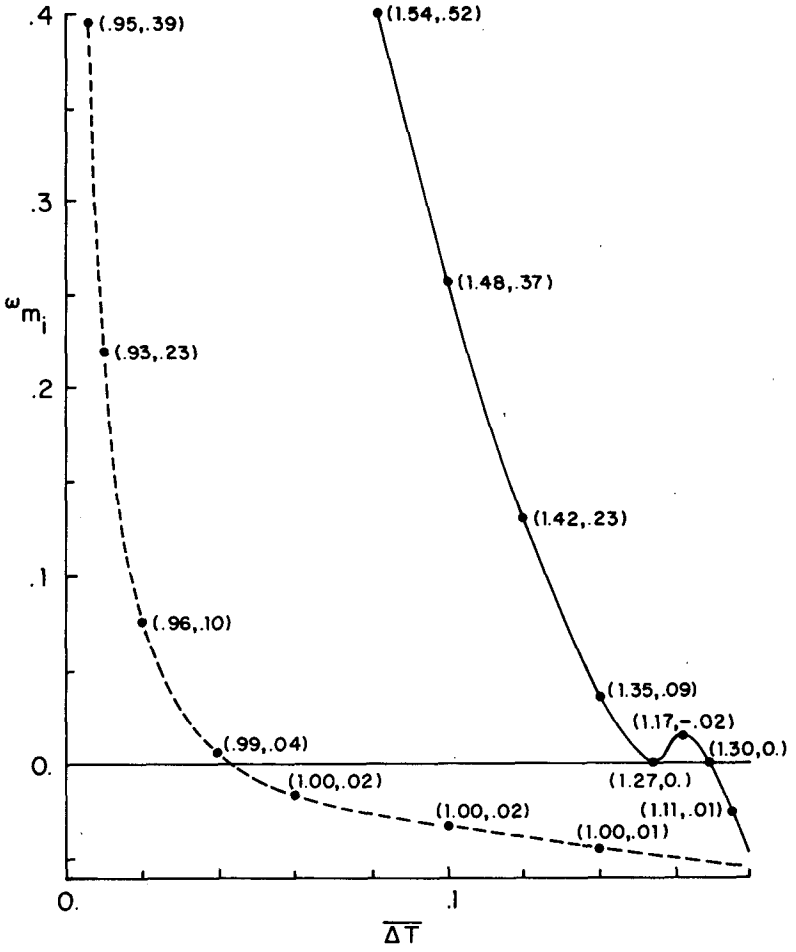

FIG. 3. ω_{m_i} vs the temperature jump ($\overline{\Delta T}$) for the short-wave instability (solid curve) for $\theta = 111°$ and $k = 3.55$ and the long wave instability (dashed curve) for $\theta = 168°$ and $k = 0.12$ with $R = \bar{h} = 2.0$, $\bar{h}_t = 0.05$, $\sigma = 1.0$, $\bar{\sigma} = 0.1$, $E = 1.0$, and complex ω in parentheses.

basic balance is given by the pair of Eqs. (14) and (15), from conditions at the interface. If we assume $\bar{h}_t = b = 0$ and that $\hat{u}_1$ is negligible, these equations yield the neutrally stable solution $\omega_m = \omega = kR\bar{u}$. If we assume $\bar{h}_t > 0$ only in (18), that is, consider only the kinematic effect of the deepening interface, we have $\omega_m = \omega + \bar{h}_t\mu = kR\bar{u}$, which after substituting for μ becomes

$$(\omega - kR\bar{u})(\omega^2 - f^2)^{1/2} = -kR\bar{h}_t. \qquad (22)$$

If we let $k = 1.0$, $R = 2.0$, $\bar{h} = 2.0$ and $\theta = \pi/2$, so that $kR\bar{u} = 1.0 = f$ and $\bar{h}_t = 0.05$, we obtain $(\omega^2 - f^2)^{2/3} = 0.1$ which has a solution $\omega = 0.89 + 0.19i$ and $\omega_m = 1$. The solution from the whole system for these parameters for $\sigma = 1000.0$ is $\omega = 0.91 + 0.19i$ and $\omega_m = 0.89 + 0.052i$. So the kinematic effect of the deepening is most important although the additional terms are necessary to make $\omega_{m_i} > 0$ and hence the system unstable. The instability is a class A instability like the unmodified ($\bar{h}_t = 0$) version as described in Part I which is destabilized by increasing friction.

This instability is of special interest because it exists for realistic values of $\overline{\Delta T} = 0.5\bar{h}$ for $\bar{h} \gtrsim 2.0$. This is shown on Fig. 7 where again the system is unstable only for $\omega_{m_i} > 0$. It is a short wavelength instability ($\sim$3 km) which is definitely realizable if K can be as large as 10^8 cm^2 s^{-1}. As mentioned in Part I, we used the value of 10^6 cm^2 s^{-1} of Brown and Owens (1982) for mesoscale in the interior which is the same value from Okubo and Ozmidov (1970) for a 100 km scale. One would expect a larger value for being in the mixed layer on the one hand but a smaller value for being a scale smaller than mesoscale on the other. So 10^6 cm^2 s^{-1} seems most reasonable, but in fact we do not know the most realistic value.

b. *Internally dominant class*

These solutions are a modification of the strongly stable internal solutions found in Kroll (1982). The basic system consists of Eqs. (6a, b) and (13c, d) with

Unauthenticated | Downloaded 01/15/25 02:54 PM UTC

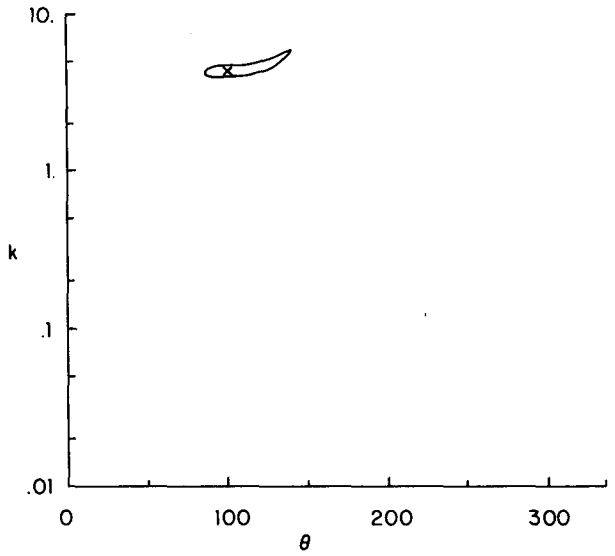

FIG. 4. The neutral contour of the mixed layer frequency ($\omega_{m_i} = 0$) in (θ, k) space for $R = \bar{h} = 2.0$, $\bar{h}_t = 0.1$, $\overline{\Delta T} = 0.2$, $\sigma = 1.0$, $\bar{\sigma} = 0.2$, and $E = 1$. At the point (×), ω_{m_i} is a maximum with $\omega_m = (2.26, 0.025)$, $\omega = (1.54, 0.13)$ and the dimensional vertical group speed minus the deepening rate is $0.024 h_* f_0$.

$b = \bar{h}_t = 0$, a self-contained system within the mixed layer independent of the interior. For a nontrivial solution for $\hat{H}$ and $\hat{T}$ in (13c, d) we must have

$$iq + 2\overline{\Delta T}[\cos\theta(U_2(0) - \langle U_2\rangle) + \sin\theta(V_2(0) - \langle V_2\rangle)]/[\bar{h}(\bar{h}\overline{\Delta T} - |\bar{\mathbf{u}}|^2)] = 0 \quad (23)$$

where $(U_2(0), V_2(0))$ from (8) and $(\langle U_2\rangle, \langle V_2\rangle)$ from (12) are from the solution of (6a, b).

This is the basic eigenvalue equation for this class. It actually has meaning only as a mathematical limit when we let $\bar{h}_t$ go to zero since any finite perturbation of $\hat{h}$ would produce unmixing and detraining which is not allowed. Thus, for physical meaning for the solution we must have $\bar{h}_t > 0$. Nonlinear effects may be important in every case but most especially in this case where, if a finite value of $\bar{h}_t + H_t$ is negative, the whole form of the equations change to prevent unmixing and detraining. Thus the realistic system for linear stability has the form of (23), modified by complicated terms of $O(\bar{h}_t)$ and $O(b)$ through which the interior enters the problem and the system radiates waves.

Let us consider special cases for (23). If $E \to \infty$, we can show that $q = 0$ and $\omega = kR\bar{u} - i\sigma k$ which is quite stable. If $E \to 0$, there is one possible unstable root derived from the equation

$$iq(q^2 - f^2) - \bar{K}(q\cos\theta + if\sin\theta) = 0, \quad (24)$$

where $\bar{K} = \overline{\Delta T}kR/(\bar{h}\overline{\Delta T} - |\bar{\mathbf{u}}|^2)$. For $\theta = \pi$, we can show that $\omega = (f^2 + i\bar{K})^{1/2} - i\sigma k^2$ and the imaginary part is given by

$$\omega_i = \{0.5[(1 + \bar{K}^2/f^4)^{1/2} - 1]\}^{1/2} - \sigma k^2. \quad (25)$$

So ω_i decreases linearly with σ and is a maximum at some k for given values of the parameters.

The system also becomes more stable for increasing E as shown on Fig. 8 derived from (23) with σ fixed at 0.1. For nominally realistic values of $K_v = 10^2$ cm^2

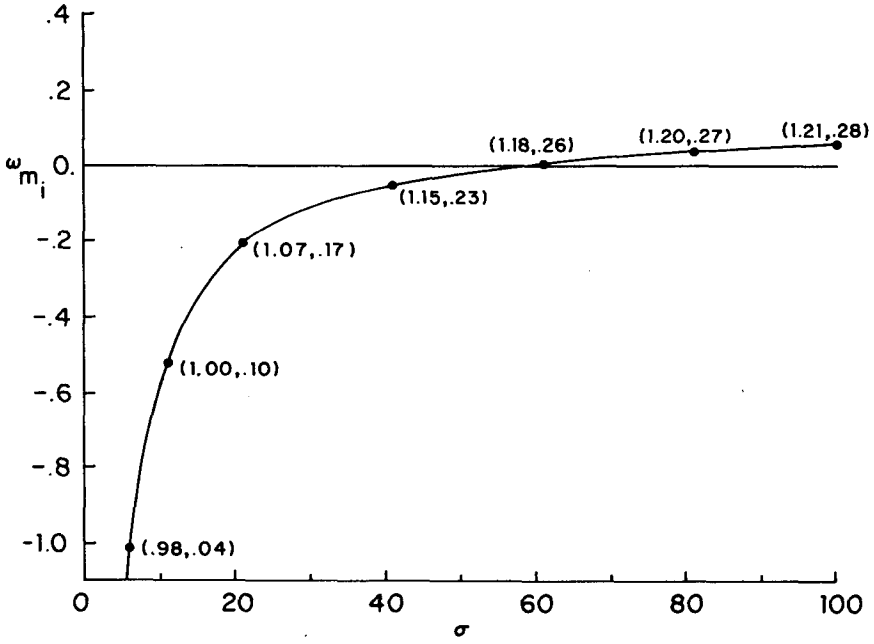

FIG. 5. ω_{m_i} vs the horizontal Ekman number (σ) for $\theta = 126°$, $k = R = \bar{h} = 2.0$, $\overline{\Delta T} = 1.0$, $\bar{h}_t = 0.1$, $\bar{\sigma} = 0.1$, $E = 1.0$, and complex ω in parentheses.

Unauthenticated | Downloaded 01/15/25 02:54 PM UTC

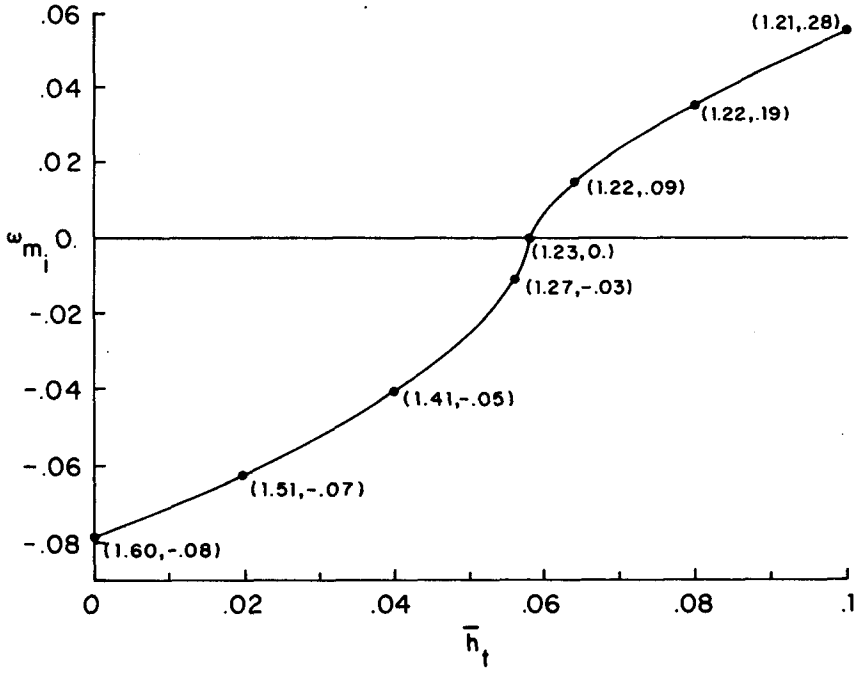

FIG. 6. ω_{m_i} vs the deepening rate ($\bar{h}_t$) for $\theta = 126°$, $k = 2.0$, $R = \bar{h} = 2.0$, $\overline{\Delta T} = 1.0$, $\sigma = 100.0$, $\bar{\sigma} = 0.2$, $E = 1.0$, and complex ω in parentheses.

s^{-1} and $K_H = 10^6$ cm^2 s^{-1} where $\sigma = E = 1.0$, the system never becomes unstable. So for instability in this case, friction must be limited. Figure 9, for $\sigma = 0.1$ ($K_H = 10^5$ cm^2 s^{-1}) and $E = 0.5$ ($K_v = 50$ cm^2 s^{-1}), shows the contours of ω_i in (θ, k) space derived from (23). The most unstable wave has a relatively short wavelength (~5 km) with a complex frequency $\omega = (1.47, 0.053)$ at an angle of 132°. It can be shown from (23) that there exists also an infinite set of stable roots.

So far we have considered only (23) derived for $\bar{h}_t = 0$. For $\bar{h}_t > 0$ we must include the complicated

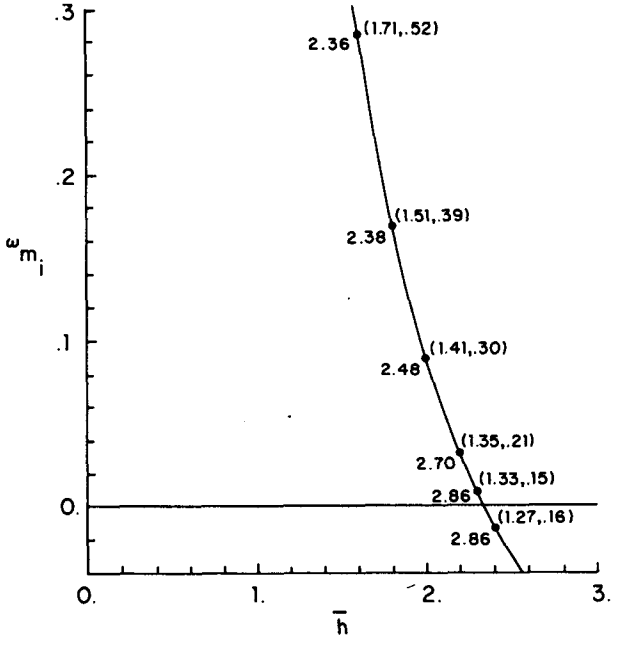

FIG. 7. The maximum value in (θ, k) space of ω_{m_i} vs the depth ($\bar{h}$) for $R = 2.0$, $\bar{h}_t = 0.5/\bar{h}^2$, $T = 0.5\bar{h}$, $\sigma = 100.0$, $\bar{\sigma} = 0.2$, and $E = 1.0$. θ is approximately 128° for all values. Complex ω is in the parentheses on the right and the dimensional wavelength in km is on the left.

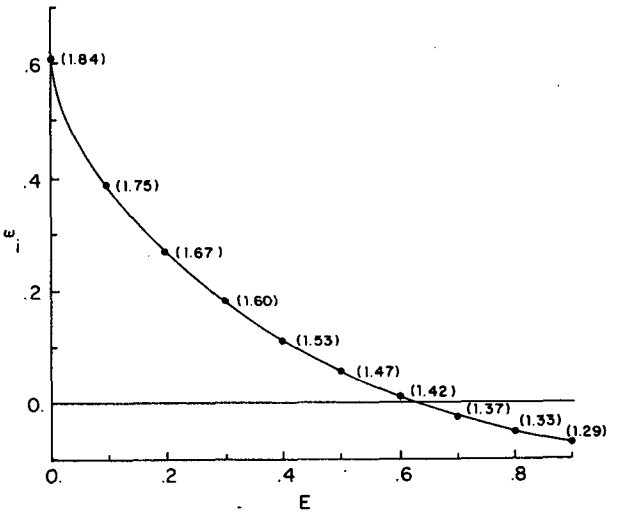

FIG. 8. $\omega_i = \omega_{m_i}$ vs the vertical Ekman number (E) for $R = \bar{h} = 2.0$, $\overline{\Delta T} = 1.0$, $\bar{h}_t = 0.0$, $\theta = 132°$, $k = 1.2$, $\sigma = 0.1$, $\bar{\sigma} = 0.0$, and real ω in parentheses.

Unauthenticated | Downloaded 01/15/25 02:54 PM UTC

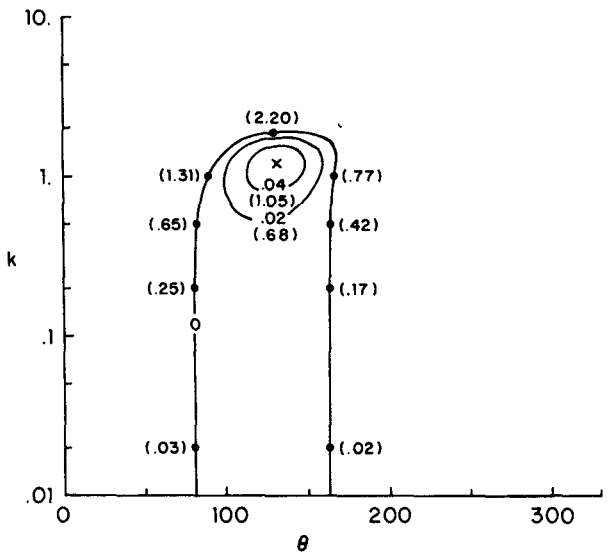

FIG. 9. Contours of $\omega_i = \omega_{m_i}$ in (θ, k) space for $R = \bar{h} = 2.0$, $\overline{\Delta T} = 1.0$, $\bar{h}_t = 0.0$, $\sigma = 0.1$, $\bar{\sigma} = 0.0$, $E = 0.5$, and real ω in parentheses. ω_i is a maximum at the point (×) where $\theta = 132°$, $k = 1.2$, and $\omega = (1.47, 0.053)$.

$O(\bar{h}_t)$ terms, in effect solving the system (13) through (20). Figure 10 shows the effect of increasing $\bar{h}_t$ from zero. Though ω_i increases, ω_{m_i} decreases with $\bar{h}_t$ and, as previously, the vertical group speed becomes less than the deepening rate at the same point where ω_{m_i} becomes negative which we again assume implies stability for the system. Figure 11 shows the variation of the maximum values of ω_{m_i} in (θ, k) space with deepening $\bar{h}$ for $\overline{\Delta T}$ and $\bar{h}_t$ varying realistically with $\bar{h}$. In this case the system actually becomes more unstable with increasing $\bar{h}$ over a certain domain, reaching a maximum, then decreasing as in all the previous cases, here and in Part I.

The salient feature of this internal instability is that it arises essentially within the mixed layer. Thus the magnitude of $\overline{\Delta T}$ is of little consequence unlike the external class of instabilities. There is no problem in having an instability for a realistic value of $\overline{\Delta T}$; however, it appears that friction must be relatively small, i.e., $K_H \approx 10^5$ cm^2 s^{-1} and $K_v \approx 50$ cm^2 s^{-1}. If conditions for an instability do exist, it has a relatively short wavelength (~5 km) and relatively strong magnitude ($\omega_{m_i} \sim 0.05$, an increase by e in 2.3 days).

6. Summary and conclusions

Clearly this system can become unstable and in various ways. It is still not clear, however, if it becomes unstable for realistic ocean conditions. The long-wave instability of Part I, which seemed likely to occur for a nondeepening mixed layer, does not seem as likely with deepening. Moreover, even if it occurs, it seems too weak to be significant. The short-wave instability of Part I, which seemed unlikely for nondeepening, seems more possible with deepening for sufficiently large horizontal friction. Paradoxically, there is a different sort of short wavelength instability (internal class) associated with deepening that is possible for sufficiently small friction.

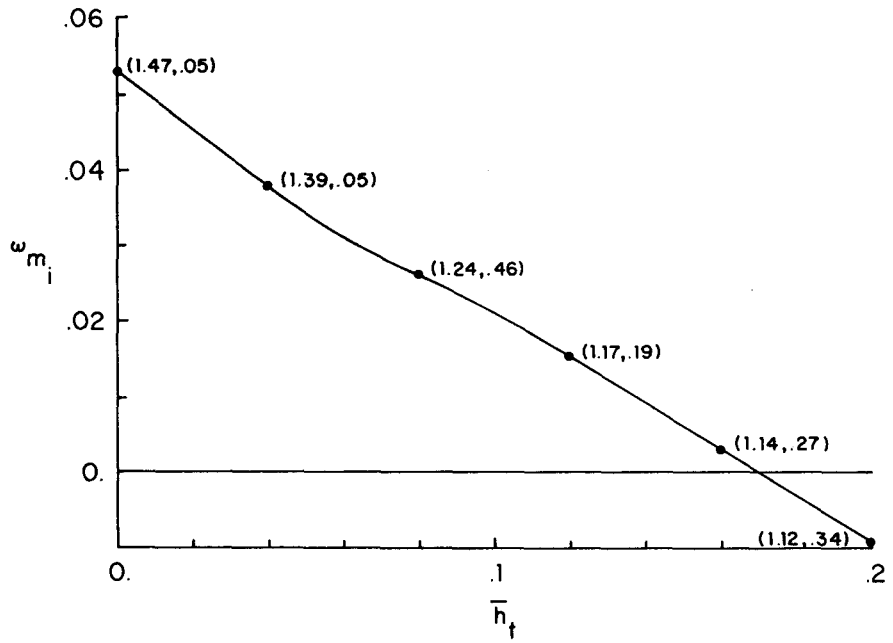

FIG. 10. ω_{m_i} vs $\bar{h}_t$ for $R = \bar{h} = 2.0$, $\overline{\Delta T} = 1.0$, $\theta = 132°$, $k = 1.2$, $\sigma = 0.1$, $\bar{\sigma} = 0.0$, $E = 0.5$, and complex ω in parentheses.

Unauthenticated | Downloaded 01/15/25 02:54 PM UTC

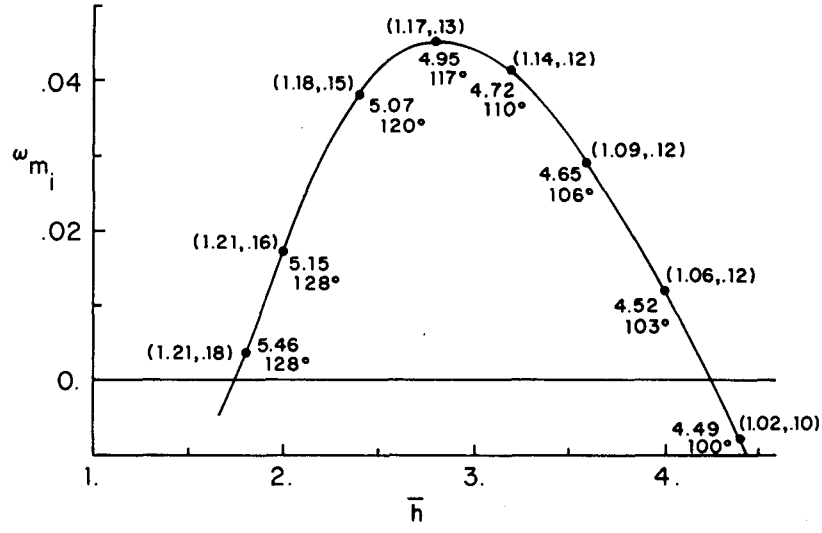

FIG. 11. The maximum value in (θ, k) space of ω_{m_i} vs $\bar{h}$ for $R = 2.0$, $\bar{h}_t = 0.5/\bar{h}^2$, $\overline{\Delta T} = 0.5\bar{h}$, $\sigma = 0.1$, $\bar{\sigma} = 0.0$, $E = 0.5$, where complex ω is in parentheses and the dimensional wavelength in km and the angle θ are under the curve.

The model and the linear stability analysis have definite limitations. It is a simple model even though the analysis becomes quite complicated. The nature of the solutions is such that the question of stability often seems to depend on the accumulation of many relatively small terms which depend on quantities such as the structure of the steady state velocity and temperature which are not modeled with any precision in the mixed layer or the interior. The analytical method is limited in that deepening and steady oscillations cannot be considered simultaneously and the transient nature of the mixed layer can only be rather simply approximated. Finally, the use of a linear stability analysis is in itself limited since nonlinear terms quite likely are as important as other secondary effects. Clearly, a numerical model would be necessary to address the foregoing limitations of the present model. Results from this study should be quite useful in constructing such a model and interpreting its results.

Acknowledgments. This work was supported by a Senior Research Associateship administered by the National Research Council at the Naval Postgraduate School, Monterey, CA.

REFERENCES

Brown, E. D., and W. B. Owens, 1982: Observations of the horizontal interaction between the internal wave field and the mesoscale flow. *J. Phys. Oceanogr.*, **11**, 1474–1481.

deSzoeke, R., 1980: On the effects of horizontal variability of wind stress on the dynamics of the ocean mixed layer. *J. Phys. Oceanogr.*, **10**, 1439–1454.

Kamachi, M., and R. Grimshaw, 1984: Over-reflection of internal–inertial waves from the mixed layer. *J. Fluid Mech.*, **141**, 179–196.

Kroll, John, 1982: An unstable uniform slab model of the mixed layer as a source of downward propagating near-inertial motion. Part I: Steady mean flow. *J. Mar. Res.*, **40**(4), 1013–1033.

——, 1987: Instability of a mixed layer model and the generation of near-inertial motion. Part I: Constant mixed layer depth. *J. Phys. Oceanogr.*, **18**, 963–976.

Niiler, P. P., 1975: Deepening of the wind-mixed layer. *J. Mar. Res.*, **33**, 405–422.

Okubo, A., and R. V. Ozmidov, 1970: Empirical dependence of the coefficient of horizontal turbulent diffusion in the ocean on the scale of the phenomenon in question. *Oceanology*, **6**, 308–309.

Stern, M. E., 1977: Interaction of the inertia–gravity waves with the wind. *J. Mar. Res.*, **35**, 479–498.

Unauthenticated | Downloaded 01/15/25 02:54 PM UTC